Fanbeam Data Consistency Conditions for Applications to Motion Detection

Rolf Clackdoyle, Simon Rit, Jan Hoskovec, Laurent Desbat

***Abstract*-- New data consistency conditions (DCC) have recently been published for fanbeam projections. We explore the potential of applying fanbeam DCC to detection and tracking of motion of a small known object inside an unknown background without the need for image reconstruction. Two scanning geometries are considered that have different data consistency properties. A downhill simplex search for 3 nonlinear parameters by minimizing inconsistency was successful. Various issues on the use of fanbeam DCC are discussed.**

I. Introduction

In image reconstruction from projections, the simple line-integral model presents a large system of linear equations. Data consistency conditions (DCC) analytically describe the redundancies in this integral equation, and they can play a useful role in image reconstruction. The idea is that by verifying the DCC of the measured data, other systematic and possibly nonlinear effects can be identified and possibly corrected before performing the tomographic reconstruction step. It was probably Natterer who pioneered this approach over 30 years ago, when he explored the use of consistency conditions on the attenuated Radon transform to identify unknown attenuation coefficients from SPECT emission measurements [Nat83]. This general approach has been followed numerous times, with a range of medical imaging applications in PET, SPECT and CT. See for example, [Nat93, Gli94, Men99, Bas00, Erl00, Pat02, Wel03, Lay05, Yu07, Tan11, Def12] among others.

At the heart of such approaches are the consistency conditions themselves. These are mathematical equations that describe the consistency (arising from redundancy) of the measurements. For the simple (non-attenuated) line-integral model which is valid for CT imaging, the well-known Helgason-Ludwig (HL) conditions [Lud66] [Hel80] apply, and are particularly useful because they can be expressed in terms of subsets of parallel projections. In other words, consistency of a sub-collection of measured projections can be checked without obtaining a full collection of projections. The situation for subsets of fanbeam projections is more complicated although such consistency conditions for linear trajectories have recently been published [Cla13].

In this work, we are only concerned with unknown density functions in the plane, and with fanbeam projections. The purpose is to explore the use of fanbeam consistency conditions and study issues that might arise in applications. We define an artificial 2D problem in motion detection which is both challenging yet within reach of fanbeam consistency methods.

II. Fanbeam Projections and Consistency Conditions

As usual in classical tomography, we let $f(x, y)$ represent the unknown density function. We define a fanbeam projection $g(v_\lambda, \cdot)$ with x-ray source at position v_λ, by

$$g(v_\lambda, \phi) = \int_0^\infty f(v_\lambda + l\alpha_\phi)dl \qquad (1)$$

where $\alpha_\phi = (\cos\phi, \sin\phi)$ with ϕ ranging over some interval of length at most 2π which may depend on the source position v_λ. The source trajectory is parameterized by $\lambda \in \Lambda$ for some bounded interval Λ. Our example trajectories will be a straight line segment, and a conventional circular scan.

Fanbeam consistency conditions can be stated for the case of a straight line trajectory that does not cut through the object. By rotating and translating the coordinate system if necessary, we can assume that the straight line trajectory is the y-axis (so $v_\lambda = (0, \lambda)$), and that the object lies entirely in the $x > 0$ half-plane. In this situation, the range of ϕ is $(-\pi/2, \pi/2)$. Now for any fixed non-negative n strictly less than the number of measured projections N, we convert each projection to a scalar function $J_n(\lambda)$ as follows:

$$J_n(\lambda) = \int_{-\pi/2}^{\pi/2} g(v_\lambda, \phi)\frac{\tan^n\phi}{\cos\phi}d\phi \qquad (2)$$

If the projections are consistent, i.e. if g satisfies equation 1 for some f, then $J_n(\lambda)$ is a polynomial in λ of degree at most n. These necessary conditions are easily verified and also turn out to be sufficient [Cla13].

The case $n = 0$ has been known in various guises for some time [Fin83, Noo02, Che05, Lev10] (see the discussions in [Tan12] and [Cla13]), and this case has the following special feature which will be relevant for the studies presented in sections III and IV below. For $n = 0$, the expression $J_0(\lambda) = \int g(v_\lambda, \phi)/\cos\phi \; d\phi$ is a constant (does not depend on λ) and the constant is given by

R. Clackdoyle is with the Laboratoire Hubert Curien, CNRS UMR 5516, Saint Etienne, France (e-mail: rolf.clackdoyle@univ-st-etienne.fr).

S. Rit is with the CREATIS laboratory, CNRS UMR 5220 and INSERM U1044, Lyon, France (e-mail: simon.rit@creatis.insa-lyon.fr).

J. Hoskovec is with the Université Jean Monnet, Saint Etienne, France (e-mail: jan.hoskovec@univ-st-etienne.fr)

L. Desbat is with the TIMC-IMAG laboratory, CNRS UMR 5525, and Joseph Fourier University, Grenoble, France (e-mail: laurent.desbat@imag.fr).

This work was partially supported by the Agence Nationale de la Recherche (France), project "DROITE," number ANR-12-BS01-0018, and partially supported by a grant from the Région Rhône-Alpes (ARC6).

$$J_0 = \iint \frac{f(x,y)}{x} dxdy \qquad (3)$$

We notice therefore that any translation of the object in the direction parallel to the trajectory line (the y direction) will not affect this constant. Furthermore, equation 3 remains constant even when replacing $f(x,y)$ by $f_1(x,y) + f_2(x,y+t)$ for any translation t of the f_2 component of f. So multiple pieces of the object translating independently in the trajectory direction also leave J_0 unchanged.

III. Materials and Methods

A. Phantom description

We used a highly simplified 2D phantom consisting of two components. The static component is a bounding elliptical shell containing 5 ellipses, and we refer to this phantom as f_1. The second component, referred to as f_2, consists of two disks undergoing motion during the simulated measurement procedure. Tables 1 and 2 give details of the ellipses making up the static and dynamic components of the phantom. Note that D_x and D_y refer to the full axis lengths of the ellipses.

For the dynamic component of the phantom, an oscillatory motion of amplitude A occurs in the horizontal direction during the time period $[t_0, t_1]$ where $0 \le t_0 < t_1 \le T$ and where T is the total duration. We take $T = 10$ seconds in this work. The precise description of the motion is given by $\Gamma_t(x,y) = (\bar{x}_t, y)$ if $t \in [t_0, t_1]$ and $\Gamma_t(x,y) = (x,y)$ otherwise, where

$$\bar{x}_t = x + \frac{A}{2}\left(1 - \cos\left(2\pi \frac{t - t_0}{t_1 - t_0}\right)\right) \qquad (4)$$

The amplitude of the motion is fixed at some value in the range $A \in [3, 9]$. The standard motion parameters used in the simulations will be $(t_0, t_1, A) = (1, 8, 7)$. The phantom is illustrated in Fig 1.

It is assumed that the static component of the phantom in Table 1 is unknown, but that the dynamic component in Table 2 is known except for the motion parameters (t_0, t_1, A). The main purpose of these experiments is to determine if the motion parameters can be extracted from projection measurements without (or before) performing image reconstruction. If the motion parameters can be determined, then a full dynamic reconstruction is possible because the moving component is then fully specified, and can be subtracted from the projections leaving the static part which can then be fed to any standard reconstruction algorithm.

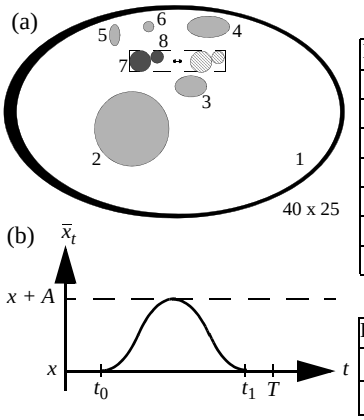

Table 1: Static Component

Ellipse	Center	(D_x, D_y)	Density
1a	(0, 0)	(40, 25)	0.5
1b	(0.5, 0)	(38, 24)	-0.5
2	(-5, -2)	(8.75, 8.75)	0.1
3	(2, 3)	(3.75, 2.5)	0.1
4	(4, 10)	(5, 2.5)	0.1
5	(-7, 9)	(1.25, 2.5)	0.1
6	(-3, 10)	(1.25, 1.25)	0.1

Table 2: Dynamic Component

Ellipse	Center	(D_x, D_y)	Density
7	Γ_t(-4, 6)	(2.5 2.5)	0.2
8	Γ_t(-2, 6.5)	(1.5, 1.5)	0.2

Fig 1. Illustration of the phantom. (a) scale drawing of the positions of the component ellipses, also showing the extent of the motion for $A = 7$. (b) plot of the motion function given by equation 4.

B. Measurement geometry 1: linogram mode

In the first measurement geometry, the x-ray source trajectory follows a straight line $v_\lambda = (\lambda, 20)$ for $\lambda \in \Lambda = [-25, 25]$. A total of 101 projections are taken along the line, starting at the position (-25, 20) and ending at (+25, 20) in steps of 0.5. The source is assumed to move at constant speed along the line, during the collection time of $T = 10$ seconds, so $\lambda = 50t/T - 25$. Each projection is considered to be instantaneously measured, with a temporal spacing of 0.1 seconds between projections.

For this geometry, a suitable range of ϕ would be $\phi \in [-\pi, 0]$, however we assume a flat immobile detector with "equispaced" sampling (in the terminology of [Kak88]) positioned along the line $y = -15$. Using the equispaced variable x_d instead of ϕ, our projection measurements become

$$\bar{g}(v_\lambda, x_d) = \int_0^\infty f(v_\lambda + l\gamma_{\lambda, x_d}) dl \qquad (5)$$

where γ_{λ, x_d} is the unit vector leaving the source at $v_\lambda = (\lambda, 20)$ and pointing at the detector position $(x_d, -15)$. To ensure that there is no truncation of these projections for the larger static phantom, the detector extent runs from (-140, -15) to (140, -15). See Fig 2(a).

When the appropriate changes of variables are applied to equation 2, we find that

$$J_n(\lambda) = \int_{-\infty}^{\infty} \cos\gamma \; \bar{g}(v_\lambda, x_d) \; (x_d)^n \; dx_d \qquad (6)$$

where γ here refers to the angle of incidence of the ray with the detector, so $\cos\gamma = 35/\sqrt{35^2 + (x_d - \lambda)^2}$.

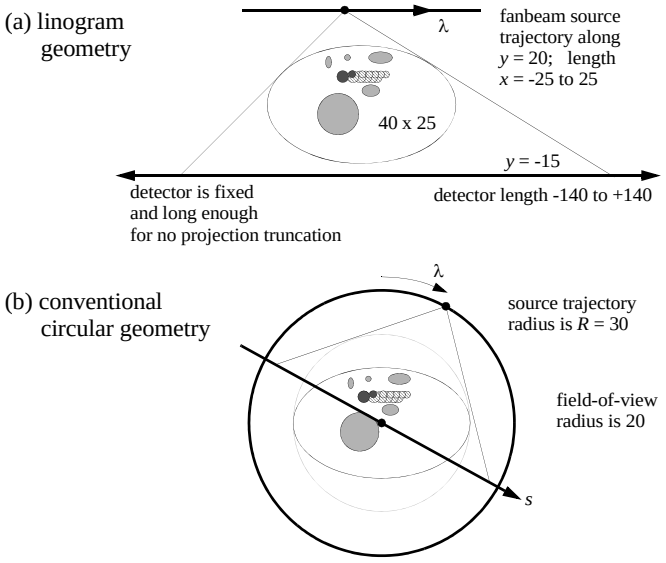

Fig 2. The two scanning geometries. (a) The linogram geometry, drawn to scale except for the extent of the detector which is long enough to avoid truncated projections. (b) The conventional circular scanning geometry.

This geometry, of parallel detector and trajectory, is the well-known linogram geometry [Edh87], and the quantity $\cos\gamma\ \bar{g}(v_\lambda, x_d)$ is a linogram. The finite length of the trajectory segment however, means that the system is tomographically incomplete so mathematically-correct image reconstruction is not possible.

The 101 linogram projections were simulated using analytic line-length calculations for the elliptical elements in the phantom, with dynamic parameters $(t_0, t_1, A) = (1, 8, 7)$ and $T = 10$ seconds. The simulated linogram is shown in Fig 3(a). Using the known dynamic component of the phantom, the unknown motion parameters (t_0, t_1, A) were sought by applying the DCC (equation 6) of orders $n = 1, 2, 3$ and calculating the residuals of the polynomial fits. If incorrect motion parameters are used to model the linogram projections, then resulting DCC may not be satisfied. Note that order $n = 0$ is not useful because the motion is parallel to the trajectory and order zero consistency is always maintained in that case.

An optimization cost function $F_n(t_0, t_1, A)$ was formed for each feasible triple (t_0, t_1, A) by simulating linograms $\bar{g}^s$ of the dynamic component of the phantom (using pixelized representations to avoid "inverse crime") and computing DCC functions $J_n^s(\lambda)$ from them according to equation 5. The difference $J_n^{\text{data}}(\lambda) - J_n^s(\lambda)$ was fit to an n-degree polynomial in λ to determine a residual vector $r_n(t_0, t_1, A)$ (recalling from equation 2 that consistency implies that $J_n(\lambda)$ is a polynomial of degree at most n). If $r_n = 0$ then the subtraction of the simulated movement from the measurement represented a consistent linogram and the unknown motion parameters were considered to be found. The cost function was defined as $F_n = \|r_n\| / \left\|J_n^{\text{data}} - J_n^s\right\|$.

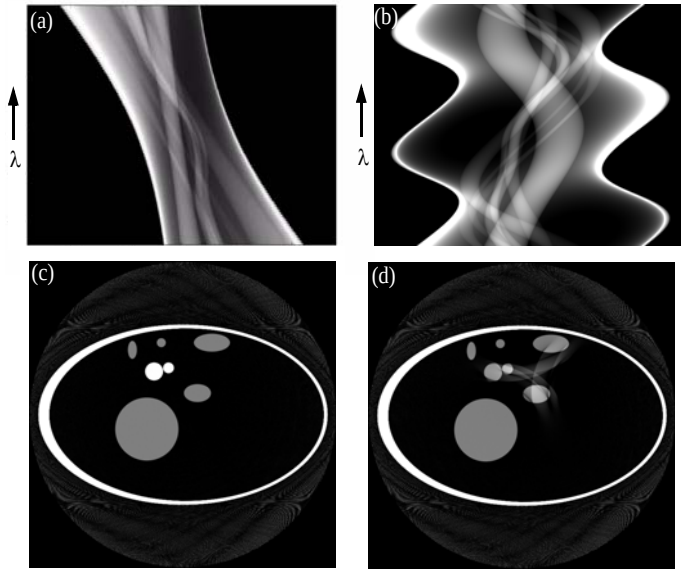

Fig 3. Top row: (a) linogram and (b) fanbeam sinogram simulations of the phantom with moving feature (more evident in linogram than sinogram). Bottom row: FBP reconstruction from (d) dynamic sinogram above and (c) from the sinogram of the frozen $t = 0$ instant of the phantom. The horizontal movement manifested itself as a triangular-shaped blurring in the reconstruction.

C. Measurement geometry 2: circular trajectory

The second fanbeam geometry is standard, consisting of 600 projections taken over a circular source trajectory of radius 30. Thus $v_\lambda = (30\sin\lambda, 30\cos\lambda)$ for $\lambda \in [0, 2\pi]$, and we note the clockwise motion of the source, starting at the "12 o'clock" position. The projections are collected at constant speed over $T = 10$ seconds, so $\lambda = 2\pi t/T$. The projections were simulated on a "virtual" flat detector passing through the origin and oriented perpendicularly to the tangent of the source motion; we use s for the detector variable. The projections are now represented by $\widehat{g}(\lambda, s) = \int_0^\infty f(v_\lambda + l\mu_{\lambda,s})dl$ where $\mu_{\lambda,s}$ is the unit vector pointing from the source to the s-position on the detector which is $(s\cos\lambda, -s\sin\lambda)$. See Fig. 2(b). The fanbeam sinogram for this 360^o circular scan is shown in Fig.3(b). Standard FBP reconstructions are shown in Figs.3(d) and 3(c) respectively for the dynamic phantom and for a static version of the phantom, frozen at $t = 0$.

For circular trajectories, fanbeam consistency can be achieved by converting an entire fanbeam dataset to parallel projections and using the standard HL conditions (e.g. [Pat01, Yu07]). Alternatively, fanbeam projections can be handled pairwise by considering the line connecting two sources as a pseudo trajectory, and applying the DCC of equation 2. With only two sources on the trajectory, only the $n = 0$ term is available (it is possible to check for equality of J_0 for two values of λ, but higher order polynomials cannot be handled). Recalling the restriction that the trajectory line not intersect the object, we find that there are a total of 96,000 pairs (pseudo trajectories).

We write $J(\lambda_i, j)$ for the DCC value corresponding to source λ_i with the (pseudo) trajectory line connecting the two sources λ_i and λ_j. Note that the cosine term in equation 2 is with respect to angle ϕ measured perpendicularly to the pseudo trajectory line. Furthermore the projection is equispaced, not equiangular (using the [Kak88] terminology) so a change of variables is needed. We skip the details of this derivation and present the final formula, which is

$$J(\lambda_i, j) = \int_{-\infty}^{\infty} \frac{\widehat{g}(\lambda_i, s)}{|R\cos(\mu/2) - s\sin(\mu/2)|} \frac{R}{\sqrt{R^2 + s^2}} ds \quad (7)$$

where $R = 30$ is the trajectory radius, and $\mu = \lambda_j - \lambda_i$ is the signed angular difference between the two source locations. Zeroth order consistency of a pair of projections simply means that

$$J(\lambda_i, j) = J(\lambda_j, i) \quad (8)$$

Note that if the line connecting sources λ_i and λ_j is horizontal then the pseudo trajectory is parallel to the motion of the dynamic component of the phantom, so even though projections λ_i and λ_j were of different temporal phases of the object, consistency of order zero is still maintained in this situation.

IV. Results and Discussion

A. The linogram scan

The cost function was calculated on a coarse grid throughout the feasible range and its behavior was studied. For order $n = 0$, it was found to be virtually constant, correctly reflecting the known theory that any horizontal motion would remain consistent for this linogram geometry. For orders $n = 1, 2, 3$ a single deep global minimum was found at the correct motion parameters as shown in the plots of Fig. 4. The few isolated local minima lay in shallow "bowls" in different locations for the different orders, suggesting that a single cost function of $F = F_1 + F_2 + F_3$ would be suitable. The cost function was re-calculated and re-examined after adding 3% Gaussian noise to the linogram data elements. The resulting plots (not shown here) were very similar except the global minimum increased slightly for $n = 1, 2, 3$.

The downhill simplex method was used for the nonlinear optimization of F_n using each of the four value of n. In each case, the routine converged in roughly 200 to 300 iterations, with the following results. For each of $n = 0, 1, 2, 3$ respectively, the estimated parameters were $(t_0, t_1, A) = (0{,}56, 9{,}97, -0{,}04)$, $(0{,}99, 8{,}01, 7{,}05)$, $(0{,}98, 8{,}00, 7{,}03)$, $(1{,}02, 8{,}00, 6{,}83)$ (recalling that the true motion parameters were $(1, 8, 7)$).

Further studies are underway, including using different true motion parameters, different initialization locations, and quantifying the effects of additive noise in the projection data.

B. The circular scan

The order zero DCC condition was calculated for every pair of source points whose connecting line (pseudo trajectory) lay outside the 20 cm field-of-view. For each pair, the percent relative difference was calculated. The results were grouped into parallel trajectory lines because the horizontal or nearly horizontal lines would not reveal inconsistency, being aligned with the movement of the dynamic component.

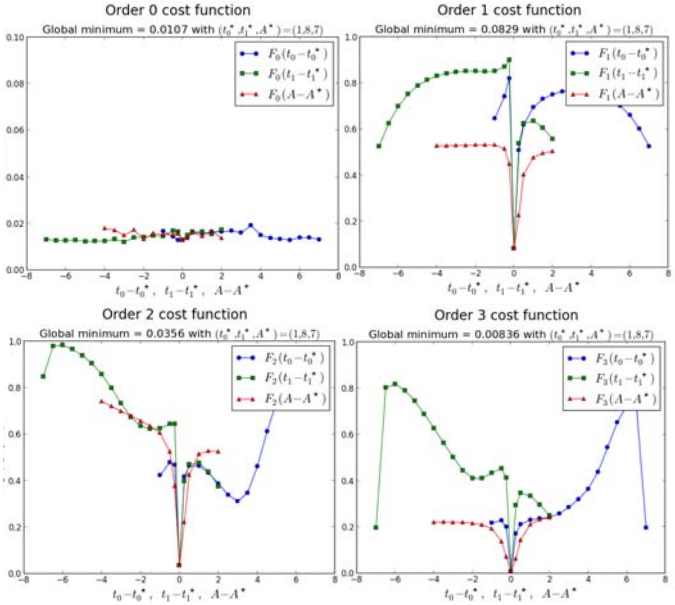

Fig 4. Perpendicular intersection plots through the global minimum of the cost function $F_n(t_0, t_1, A)$ for each of $n = 0$ (top left); $n = 1$ (top right); $n = 2$ (bottom left); $n = 3$ (bottom right). The vertical scale for $n = 0$ is magnified 10 times with respect to the other three scales. The plots illustrate the abrupt fall of the cost function in the immediate neighborhood of the true motion parameters.

At a fixed orientation, there were always 160 parallel trajectory lines, 80 on each side of the field-of-view (FOV). These lines varied from 20 cm to 30 cm from the center of the system. We grouped the lines as shown in Fig 5, and displayed the *average* percent relative difference over all the parallel lines lying on one side of the FOV. We also plotted the average relative difference for just the lines between 20 cm and 25 cm from the center, because they represent source pairs that are more separated temporally: from 1.83 second minimal separation to 2.67 seconds of separation, whereas consecutive sources are only separated by 0.017 seconds. (For the pairs of source positions that cross the starting point, the lines between 20 cm and 25 cm from the center respectively have temporal separation between 8.17 and 7.33 seconds.)

The results of the graph show two effects. One is that, as predicted by the theory, the horizontal (0^o or 180^o) movement does not cause inconsistency, because horizontal and nearly horizontal trajectory lines showed very low relative differences. The other effects are due to temporal behavior of the phantom. Each condition compares one pair of snapshots and there are many instances when the phantom can be in the same position for the two snapshots. The 1 second immobile period at the start and the 2 seconds at the end maintain consistency during these periods, as do snapshots that are temporally symmetric about the midpoint of the motion, which occurs at $t = 4.5$ seconds. The flat region in Fig 5 near 160 degrees is attributed to this symmetry effect.

We note that the average relative errors appear quite small, all under 0.5%, but it is important to note that the mass of the moving part of the phantom is a small fraction of the total.The total number of lines (conditions $J(\lambda_i, j) = J(\lambda_j, i)$) in this simulation was 96000. These conditions could be exploited in a similar way to those of the linogram to provide estimates of the motion parameters.

The flat areas of the plot of Fig 5 can be used to roughly identify the *direction* of the motion, because a strictly linear motion will enforce two angles, separated by 180 degrees, for which consistency will generally hold.

V. Summary and Conclusions

With two different fanbeam geometries, various features of the application of DCC have been explored. The order zero condition can not detect motion parallel to the trajectory, but can potentially be used to detect the direction of linear movement. In our simulations, the higher order conditions could be used to build a suitable cost function for finding three motion parameters for a simple motion of a known component of the phantom. The DCC are linear in the components of the image, so they might become swamped if a large static background object were involved. There are many potential applications of fanbeam DCC, and we have illustrated various approaches and and discussed their features and limitations.

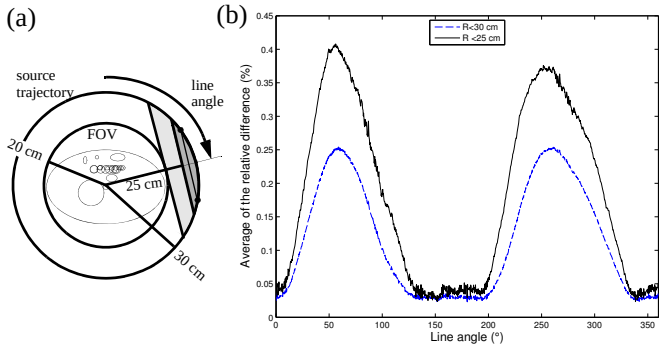

Fig 5. Average relative differences. (a) illustration of a group of parallel trajectory lines showing the $R < 30$ cm group (shaded) and $R < 25$ cm group (light shading). (b) Plot of average relative difference as a function of line angle for all lines (lower curve) and for just those lines closer than 25 cm (upper curve).

VI. References

[Bas00] S. Basu and Y. Bresler. "Uniqueness of tomography with unknown view angles." *IEEE Trans Imag Proc* 9, 1092-1106, 2000.

[Che05] G.-H. Chen and S. Leng. "A new data consistency condition for fan-beam projection data." *Med Phys* 32, 961-967, 2005.

[Cla13] R. Clackdoyle. "Necessary and Sufficient Consistency Conditions for Fanbeam Projections along a Line." *IEEE Trans Nucl Sci*, 60, 1560-1569, 2013.

[Def12] M. Defrise, A. Rezaei and J. Nuyts. "Time-of-flight PET data determine the attenuation sinogram up to a constant." *Phys. Med. Biol.* 57, 885-899, 2012.

[Edh87] P.R. Edholm and G.T. Herman. "Linograms in image reconstruction from projections." *IEEE Trans. Med. Imag.* MI-6, 301–307, 1987.

[Erl00] K. Erlandsson, D. Visvikis, W.A. Waddington and P. Jarritt. "Truncation Reduction in Fan-Beam Transmission Scanning Using the Radon Transform Consistency Conditions." *IEEE Trans. Nuc. Sci*. 47, 989–993, 2000.

[Fin83] D.V. Finch and D.C. Solmon. "Sums of homogeneous function and the range of the divergent beam X-ray transform." *Numer Func Anal and Optimiz* 5, 363–419, 1983.

[Gli94] S.J. Glick, B.C. Penney, M.A. King and C.L. Byrne "Noniterative Compensation for the Distance-Dependent Detector Response and Photon Attenuation in SPECT Imaging" *IEEE Trans.Med. Imag*. 13, 363–374, 1994.

[Hel80] S. Helgason. *The Radon Transform.* (Boston: Birkhauser), 1980.

[Kak88] A.C. Kak and M. Slaney. *Principles of Computerized Tomographic Imaging* (New York: IEEE Press) 1988.

[Lay05] C.M. Laymon, M. Swadley, J.E. Bowsher, T. Blodgett and S.K. Ziolko. "Evaluation of Sinogram Consistency Conditions for Identifying Artifactual PET Attenuation Images". *Conf Rec of the 2005 Nucl Sci Symp and Med Imag Conf.* 3, 1611-1614, 2005.

[Lev10] M.S. Levine, E.Y. Sidky and X. Pan. "Consistency Conditions for Cone-Beam CT Data Acquired with a Straight-Line Source Trajectory." *Tsinghua Sci Technol* 15,56–61, 2010.

[Lud66] D. Ludwig. "The Radon transform on Euclidean space." *Comm. Pure Appl. Math.* 19, 49–81, 1966.

[Men99] C. Mennessier, F. Noo, R. Clackdoyle, G. Bal and L. Desbat. "Attenuation correction in SPECT using consistency conditions for the exponential ray transform." *Phys. Med. Biol*. 44, 2483–2510, 1999.

[Nat83] F. Natterer. "Computerized tomography with unknown sources." *SIAM J. Appl. Math*. 43, 1201-1212, 1983.

[Nat93] F. Natterer. "Determination of tissue attenuation in emission tomography of optically dense media." *Inv. Probs* 9, 731–736, 1993.

[Noo02] F. Noo, M. Defrise, R. Clackdoyle and H. Kudo. "Image reconstruction from fan-beam projections on less than a short scan." *Phys. Med. Biol*. 47, 2525-2546, 2002.

[Pat01] S.K. Patch. "Moment conditions indirectly improve image quality." Contemp. Math. 278, 193-205, 2001.

[Pat02] S.K. Patch. "Consistency conditions upon 3D CT data and the wave equation." *Phys. Med. Biol*. 47, 2637-2650, 2002.

[Tan11] S. Tang, X. Mou, Q. Xu, Y. Zhang, J. Bennett and H. Yu. "Data consistency condition-based beam-hardening correction." *Opt. Eng.* 50, 076501(1–13), 2011.

[Tan12] S. Tang, Q. Xu, X. Mou and X. Tang. "The mathematical equivalence of consistency conditions in the divergent-beam computed tomography." *J. X-ray Sci. Tech*. 20, 45-68, 2012.

[Wel03] A. Welch, W. Hallett, P. Marsden and A. Bromiley "Accurate Attenuation Correction in PET using Short Transmission Scans and Consistency Information." *IEEE Trans Nucl Sci* 50, 427–432, 2003.

[Yu07] H. Yu and G. Wang. "Data Consistency Based Rigid Motion Artifact Reduction in Fan-Beam CT." *IEEE Trans. Med. Imag*. 26, 249–260, 2007.